ELSEVIER

J. Non-Newtonian Fluid Mech. 118 (2004) 33–48

Journal of Non-Newtonian Fluid Mechanics

www.elsevier.com/locate/jnnfm

Turbulent pipe flow of shear-thinning fluids

M. Rudman*, H.M. Blackburn, L.J.W. Graham, L. Pullum

CSIRO Manufacturing and Infrastructure Technology, PO Box 56, Highett 3190, Australia

Received 27 December 2002; received in revised form 7 February 2004

Abstract

Direct numerical simulation of the weakly turbulent flow of non-Newtonian fluids is undertaken for two different generalised Newtonian rheology models using a spectral element-Fourier method. Results for a power law (shear-thinning) rheology agree well with experimentally determined logarithmic layer correlations and with other previously published experimental work. As the flow index becomes smaller for the same Reynolds number, the flow deviates further from the Newtonian profile and the results suggest that transition is delayed. Predicted friction factors fall above those in the literature, but below the Newtonian values when a comparison is undertaken on the basis of the Metzner–Reed Reynolds number. Results for a Herschel–Bulkley model (yield stress + shear-thinning) are compared to corresponding experimental measurements and are found to be in very good agreement. Use of direct numerical simulation shows great promise in understanding transition and turbulence in non-Newtonian fluids.

Keywords: Direct numerical simulation (DNS); Non-Newtonian; Pipe flow; Turbulence; Transition; Shear-thinning; Friction factor

1. Introduction

The flow of non-Newtonian fluids and slurries in pipes occurs in a wide range of practical applications in the process industries. If the fluid has a significant yield stress, or if its effective viscosity is high, industrially relevant flow rates may occur in the laminar flow regime (e.g. for thickened slurry discharge in the minerals industry). However, in some cases the flow can be turbulent and there are advantages in operating pipe flows in a transitional flow regime because the specific energy consumption is lowest there. In the case of solids transport, the flow structures associated with intermittency may be used to keep particles in suspension without the much higher pressure losses of the fully turbulent regime. Although some experimental work has appeared on the transitional and turbulent flow of non-Newtonian fluids, [1–3], little fundamental understanding exists. General theories of turbulence are lacking for non-Newtonian fluids, and the development of mathematical and computational models is not well advanced.

Computational modelling of non-Newtonian flows, especially using direct numerical simulation (DNS), shows promise in helping to understand transition and turbulence in these fluids. The main benefit of using a DNS technique is that once validated, it can be reliably used to model the flow behaviour and provide a detailed picture of turbulent structure. Such a picture is difficult to obtain experimentally in optically clear laboratory fluids, and almost impossible to obtain in opaque, fine particle suspensions. DNS has the added benefit that other rheological effects such visco-elasticity that can arise in laboratory fluids (but not real suspensions) do not have to be considered in the model. The effects of modifying individual rheological parameters can also be easily isolated in a simulation, whereas they are often coupled in real fluids. In addition, the technique also allows the validity of rheological models to be assessed in different flow scenarios.

There have been some DNS of the turbulent flow of polymer solutions with the aim of understanding the causes of drag reduction (e.g. [4–7]). In those studies, dilute polymer solutions were considered in which shear-thinning behaviour was negligible and elongational (visco-elastic) effects were taken into account using various methods for the extra elastic stresses. However, for a wide range of important materials, the non-Newtonian rheology is primarily of a shear-thinning nature and visco-elastic effects are negligible. Malin [8] considered turbulent pipe flow of power law fluids using a Reynolds-averaged approach and a

* Corresponding author.
E-mail address: murray.rudman@csiro.au (M. Rudman).

0377-0257/$ – see front matter © 2004 Elsevier B.V. All rights reserved.
doi:10.1016/j.jnnfm.2004.02.006

modified k–ϵ model. Reasonable agreement with experimental data was obtained after modifying the wall damping functions, however, this approach is at least in part empirical, and does not shed light on the fundamental flow effects arising from shear-thinning behaviour. Apart from some recent work [9,10] there have been few published computational investigations of turbulent flows of shear-thinning non-Newtonian fluids without visco-elasticity.

Experimental results show that, compared to Newtonian fluids, the transition to turbulence may be delayed in shear-thinning fluids (i.e. it occurs at a higher generalised Reynolds number) [1,10]. There is also evidence that the radial and azimuthal turbulence intensities are lower by 20–40% for a power law fluid compared to a Newtonian fluid, whereas the axial intensities may be marginally higher [1–3]. The aim of the present study is to investigate the effect of rheological parameters and to consider the modification to the flow that arises in the presence of a fluid yield stress.

1.1. Rheology models

The fluids modelled in this study are shear-thinning non-Newtonian fluids whose rheology is described by a generalised Newtonian model, i.e. one in which an isotropic viscosity dependent on flow properties is applicable. In the present work, particular fluids are considered in which the viscosity η can be described using either the power law (Ostwald–de Waele) model:

$$\eta = K\dot{\gamma}^{n-1}, \tag{1}$$

or the Herschel–Bulkley model

$$\eta = \frac{\tau_y}{\dot{\gamma}} + K\dot{\gamma}^{n-1}, \tag{2}$$

where $\dot{\gamma}$ is the shear rate, K the consistency, n the flow index, and (in the case of the Herschel–Bulkley model) τ_y the yield stress. In the case of the power law model, $n < 1$ for shear-thinning, $n = 1$ for Newtonian, and $n > 1$ for shear-thickening fluids. The shear rate is computed from the rate-of-strain tensor $\vec{S}$ as

$$\dot{\gamma} = (2\vec{S} : \vec{S})^{1/2}. \tag{3}$$

1.2. Generalised Reynolds number

When the viscosity varies in space and time, the appropriate viscosity scale to use in order to define a Reynolds number is not obvious. There are a number of possible choices:

(1) The zero shear viscosity. This is used in [5,6] for DNS of visco-elastic flows, however, it is not appropriate for the power law and Herschel–Bulkley models as it is infinite.
(2) The average viscosity. This value on first inspection appears reasonable, however, it is not known a priori and requires an iterative procedure of running simulations, modifying parameters, etc. More importantly, based on results discussed below, the consequences of using such a viscosity scale are:
   - The near-wall scaling is no longer $U^+ = y^+$;
   - The value of the Reynolds number for flows that are transitional and weakly turbulent falls below the Newtonian transitional Reynolds number of 2100 for some fluids;
   - The turbulence statistics do not collapse as neatly.

   These points suggest that this viscosity scale is not appropriate.
(3) The mean centreline viscosity is not applicable for the same reasons as the average viscosity.
(4) The mean wall viscosity.

The choice made here is to use a mean wall viscosity, η_w. The mean wall viscosity can be determined a priori. It is calculated from the mean wall shear stress, τ_w, that in turn is determined directly from the applied axial pressure gradient:

$$\tau_w = \frac{D}{4}\frac{\partial p}{\partial z}. \tag{4}$$

Assuming a Herschel–Bulkley rheology, it is straightforward to show that

$$\eta_w = K^{1/n}\frac{\tau_w}{(\tau_w - \tau_y)^{1/n}}. \tag{5}$$

For the power law model, τ_y is set to zero in Eq. (5). The resulting generalised Reynolds number used here is then based on the pipe diameter D, superficial (or bulk) velocity ($\bar{U}$), the fluid density (ϱ), and η_w

$$Re_g = \frac{\varrho \bar{U} D}{\eta_w}. \tag{6}$$

It should be noted that this Reynolds number has been used by others [1,11,12] and has been shown to suitably collapse data for the flow of non-Newtonian fluids. However, because the mean viscosity varies in the flow, so will local estimates of Reynolds number. Consequently, Re_g will not completely specify the governing dynamics of the flow.

The generalised Reynolds number used here (Eq. (6)) is different to the more traditional Metzner–Reed Reynolds number that, for a power law fluid, can be written in closed form as

$$Re_{MR} = \frac{8\varrho \bar{U}^{2-n} D^n}{K(6 + 2/n)^n}. \tag{7}$$

(For fluids other than power law fluids, Metzner–Reed Reynolds number can also be calculated, see for example [13].) The generalised Reynolds number, Re_g, reflects flow behaviour in the near-wall region that plays a fundamental role in transition and the development of turbulence in wall bounded flows of Newtonian fluids. As such, it is believed that this is a more suitable basis on which to compare and order simulation results.

1.3. Law of the wall scaling

Wall units are introduced in a similar manner to the Newtonian analysis with the wall viscosity (η_w) taking the place of the Newtonian viscosity. Hence the friction velocity is defined as $u_\tau = \sqrt{\tau_w/\varrho}$, the non-dimensional velocity is $U^+ = U/u_\tau$ and the non-dimensional distance from the wall is written as $y^+ = (\varrho u_\tau/\eta_w)(r - R)$, where R is the pipe radius.

2. Numerical method

The spatial discretisation employs a spectral element-Fourier formulation, which allows arbitrary geometry in the (x, y) plane, but assumes periodicity in the z (axial, or out-of-plane) direction [14]. A second-order-in-time mixed explicit–implicit technique [15] is employed for time integration of the incompressible momentum equations, which for a spatially variable viscosity η read as

$$\partial_t \vec{u} + \vec{N}(\vec{u}) = -\frac{1}{\varrho}\nabla p + \frac{1}{\varrho}\nabla \cdot [\eta\{\nabla\vec{u} + (\nabla\vec{u})^T\}],$$
$$\nabla \cdot \vec{u} = 0. \quad (8)$$

The non-linear terms $\vec{N}(\vec{u})$ are implemented in skew-symmetric form, i.e. $\vec{N}(\vec{u}) = (1/2)(\vec{u}\cdot\nabla\vec{u} + \nabla\cdot\vec{u}\vec{u})$ as this has been found to reduce aliasing errors.

To allow a semi-implicit treatment of the viscous terms, the non-Newtonian viscosity is decomposed into a spatially constant component, η_r, and a spatially varying component $\eta - \eta_r$. The spatially varying component is treated with a second-order explicit formulation and the constant component is treated implicitly, thus enhancing the overall numerical stability of the scheme [16]. The basic concept is to ensure that the reference viscosity is larger than the local (varying) viscosity throughout most of the domain, most of the time. This results in the explicitly treated terms utilising a negative viscosity most of the time. An initial estimate of the reference viscosity η_r is chosen to be the viscosity at a shear rate equal to the superficial flow velocity divided by the pipe radius. This value is not known exactly a priori, but can be estimated. If the value of η_r leads to numerical instability, it can be adjusted during the computation without adverse effects. Too small a value of η_r will lead to most of the viscosity being treated explicitly with either stability problems or very small time steps. Choosing too large a value also leads to instability for reasons that are not clearly understood. In practice it is found that η_r should be decreased as n decreases, and (for example) the initial estimate was halved for the $n = 0.5$ simulation. It should be noted that the reference viscosity η_r is a numerical construction and is not explicitly related to the physics of the flow. In particular, it should not be confused with the wall viscosity.

Because both the power law and Herschel–Bulkley rheology models have a singular viscosity at zero shear rate, a 'cut-off' value is used, below which the shear rate is assumed to be constant when computing the viscosity. The cut-off value is chosen to be 10^{-5} times the mean shear rate and its use is not observed to cause any stability problems or significant errors. Although no statistics have been gathered, instantaneous field dumps for both the power law and Herschel–Bulkley fluids have never been observed to contain shear rates below the cut-off. The smallest value is often several orders of magnitude higher than this, even in the less active core regions of the flow, hence it is believed that the cut-off is almost never invoked in practice.

In order to drive the flow in the axial (z) direction, a body force per unit mass equivalent to the pressure gradient measured in the experiments is applied to the z-momentum equation. This approach allows the pressure to be periodic in the axial direction.

The planar/Fourier representation of three spatial dimensions leads naturally to parallel implementations in which for most of the time step each process carries a subset of two-dimensional complex modes. The non-linear terms $\vec{N}(\vec{u})$ are formed pseudospectrally with the aid of interprocess memory exchanges. These exchanges are implemented using the message-passing kernel (MPI), and the computations reported here were carried out using 16, 24 or 32 processors on the Australian Partnership for Advanced Computing (APAC) National Facility cluster. Run times were typically in the order of 2000 CPU hours to reach a statistically steady state, with an additional 500–1000 CPU hours used to obtain statistics. These latter times corresponded to 30–60 fluid transit times over the length of the computational domain.

2.1. Computational parameters

The simulations here were originally designed to allow comparison to experiments undertaken in a 105 mm pipe test loop (see [10]) and the parameters were chosen to match with these experiments. The computational domain consists

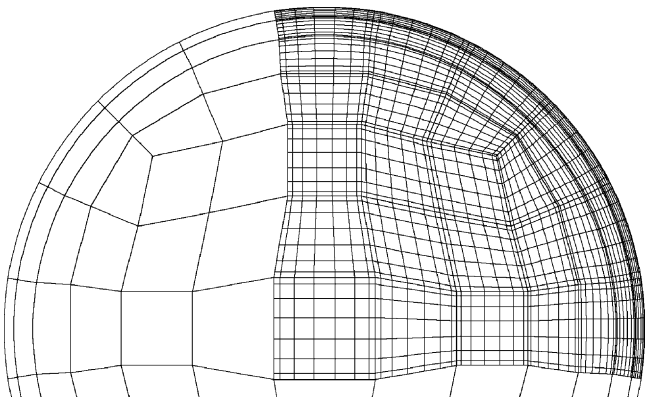

Fig. 1. Upper part of the two-dimensional mesh cross-section showing spectral element boundaries and node points (the nodal mesh is shown on the right side only). Fourier expansions with 80–128 modes (160–256 planes) were used in the axial direction.

Table 1
Parameters for simulations reported here: 'length' is the axial periodic length of the domain, while 'modes' is the number of Fourier modes employed in the pipe-axis direction, and $\partial p/\partial z$ is the axial pressure gradient (Pa/m) used to drive the flow

Model	n	K	τ_y (Pa)	$\partial p/\partial z$	Re_g	Re_{MR}	Length	Modes
Power law	0.5	1.527	–	1441	5339	2975	$4\pi D$	128
Power law	0.5	1.527	–	1441	5252	2936	$8\pi D$	256
Power law	0.69	0.483	–	1695	5501	3636	$5\pi D$	108
Power law	0.75	0.320	–	1745	5514	3935	$4\pi D$	108
Herschel–Bulkley	0.52	1.203	1.35	1420	5800	3025	$4\pi D$	80
Herschel–Bulkley	0.52	1.203	1.35	1725	8130	3840	$4\pi D$	80

of 105 eighth-order elements in the pipe cross-section (see Fig. 1) and (with the exception of one simulation) 80–128 Fourier modes (i.e. 160–256 data planes) in the axial direction, with domain lengths of 4–5πD depending on Reynolds number and flow index. A summary of the simulation parameters is provided in Table 1. One simulation was re-run on a domain length of $8\pi D$ with 256 Fourier modes to consider domain length effects.

In terms of wall units, the near-wall mesh spacing is $y^+ \approx 0.5$, $R\theta^+ \approx 8$ and $z^+ \approx 35$. This resolution is perhaps marginal in the streamwise direction, although a grid convergence study discussed later suggests that significantly increasing the streamwise resolution had little effect on the turbulence statistics, and is therefore sufficient for this initial investigation.

In order to maintain a uniform generalised Reynolds number in the power law simulations, as n was changed both the consistency, K, and the driving pressure gradient were altered to maintain the same wall viscosity and superficial velocity. A similar process was used in the Herschel–Bulkley simulations where the yield stress was also kept constant. This variation of parameters was achieved using the correlations between pressure gradient and superficial velocity for power law and Herschel–Bulkley fluids due to Wilson and Thomas [17].

2.2. Validation

The underlying numerical code has been validated for both DNS and LES of pipe and channel flow [18–20]. The implementation of the power-law non-Newtonian viscosity was validated against laminar pipe flow and axisymmetric Taylor–Couette flow of power-law fluids, both of which have analytic solutions. For the Herschel–Bulkley model, validation was against laminar pipe flow only. In all cases, numerical and theoretical velocity profiles agreed to within 0.01% and the code is believed to accurately predict the flow of non-Newtonian fluids with generalised Newtonian rheologies.

To check the grid independence of the turbulent flow solutions, the simulation at $n = 0.69$ was run at three different resolutions. A coarse resolution given by 80 Fourier modes (i.e. 160 z-planes) and 105 6×6 elements, a medium resolution (at which the simulations reported here are undertaken) of 108 Fourier modes and 105 8×8 elements and a fine mesh with 192 Fourier modes and 189 8×8 elements. The mean velocity profiles were almost indistinguishable from each other. The turbulence intensities and Reynolds stresses are shown in Fig. 2. Clearly, the results for the coarse mesh lie approximately 5% below the other results for the turbulence intensities, although they agree well for Reynolds stress. The difference between the medium and fine mesh results are insignificant, justifying the use of the medium size mesh for the simulations reported here.

2.2.1. Discussion of earlier validation results

In [9,10], DNS simulations of a 0.6 wt.% carboxymethylcellulose (CMC) solution were undertaken using a power law rheology model with $n = 0.69$. The simulation results were compared to turbulent flow experimental data for this fluid in an attempt to validate the predictions of the model. Those results are presented again here in Fig. 3 and are for a (nominal) value of $Re_g = 4680$.

It is seen that a significant disagreement between simulation and measurement exists. Not only is the predicted

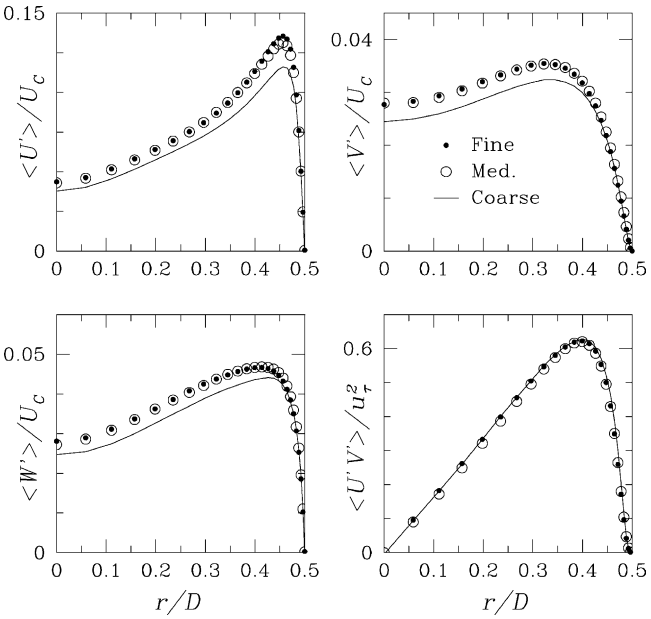

Fig. 2. Dependence of turbulence statistics on grid resolution. Axial, radial and azimuthal turbulence intensities and Reynolds stresses for power law simulations undertaken at fine, medium and coarse resolutions for $n = 0.69$, $Re_g = 5500$. See text for further description.

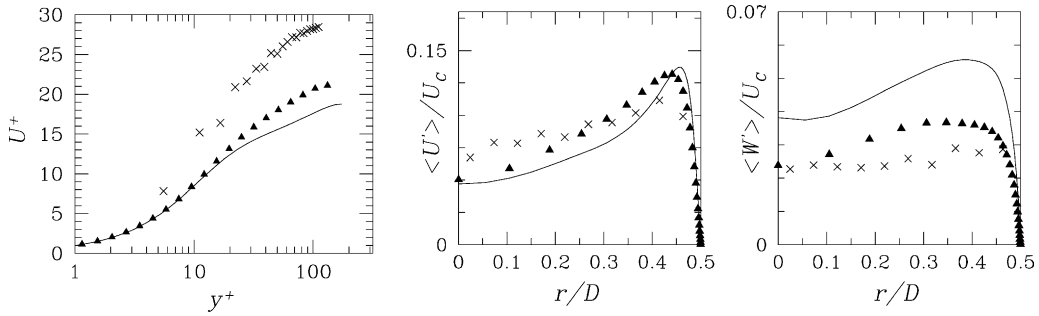

Fig. 3. Mean axial velocity profiles and turbulence intensities for the turbulent flow of a 0.6 wt.% CMC solution discussed in [9,10]. (×) experiment, (▲) simulation, solid line is Newtonian profile at $Re = 5500$.

superficial velocity approximately 25% lower than experiment, but the (non-dimensionalised) velocity profile has a significantly different shape to the experimental profiles. The simulation is suggestive of a turbulent profile, whereas the experiment appears to be transitional.

This experimental result for CMC is consistent with previously reported observations. In [13] experimental results for a 0.3 wt.% CMC solution were observed to exhibit anomalous behaviour when compared to other shear-thinning fluids, and were not included in the subsequent analysis—visco-elasticity was cited as the most likely reason. Rheology measurements and turbulent pipe flow measurements of 0.25–0.4 wt.% CMC solutions in [3] suggest that first normal stress differences become significant at concentrations higher than approximately 0.2 wt.% and will result in drag reduction as a result of visco-elastic effects. The observed drag reduction in [3] is consistent with the discrepancy between experiment and DNS seen in Fig. 3.

In contrast to results in [3], independent rheological tests undertaken on a 0.6 wt.% CMC solution showed no firm evidence of first normal stress differences over a range of shear rates applicable to the experiments. Although attribution of the discrepancy above to visco-elastic effects in CMC is tempting, this cannot be done with any certainty and its cause remains unknown. Given that anomalous behaviour has been previously observed in CMC solutions (compared to other nominally power law fluids), the discrepancy is not surprising, however, strict validation of the turbulent power law simulations remains elusive. Although *unvalidated*, the results are not believed to be *invalidated* by this discrepancy for the reasons outlined above.

The discrepancy between simulation and experiment highlights the difficulty in modelling polymer solutions using simple rheological models such as a power law model. Although the power law model may be valid over limited ranges of shear rates and can give quite accurate results when used to simulate laminar flows, its usefulness in turbulent flow where shear rates may span many decades is less easily determined. Regardless of this difficulty, the effect of modifying shear-thinning parameters is of fundamental interest and is considered below. Instead of comparing to experimental results for CMC, the numerical results will be compared to available experimental correlations from the literature.

3. Results

The results from six simulations are presented here—four simulations for power law fluids at a generalised Reynolds number of approximately 5500 and two simulation of a Herschel–Bulkley fluid at generalised Reynolds numbers of 5800 and 8130. For the power law simulations, three different power law indices were considered (see Table 1) and the pressure gradient in each case was modified to keep Re_g as close to 5500 as possible. The case of $n = 0.5$ was run at two different domain lengths. For the Herschel–Bulkley simulations, parameters were chosen to give results that were comparable to unpublished experimental measurements.

Although simulations are undertaken in a Cartesian coordinate system, all results are presented in a cylindrical coordinate system in which the axial velocity is denoted by U, the radial velocity by V and the azimuthal velocity by W.

3.1. Power law fluids

3.1.1. Mean flow profiles for power law fluids

The mean axial velocity for the three simulations at $Re_g \approx 5500$ for $n = 0.5$, 0.69 and 0.75 are shown in Fig. 4. They are plotted with conventional 'Law of the wall' non-dimensionalisation and are compared to a Newtonian velocity profile for pipe flow at $Re = 5500$ calculated using the same DNS code. As the index n increases, the profiles for the power law fluids approach the Newtonian profile, as expected. The results for $n = 0.5$ fall sufficiently above the Newtonian profile to suggest that this flow might be transitional—this point will be discussed in more detail below.

In [21], Clapp reports the results of experimental measurements of the turbulent pipe flow of power law fluids with flow indices in the range 0.698–0.813. Based on these measurements, dimensional arguments, and other measurements of turbulent Newtonian pipe flow reported in [22], Clapp determines that the logarithmic velocity profile for

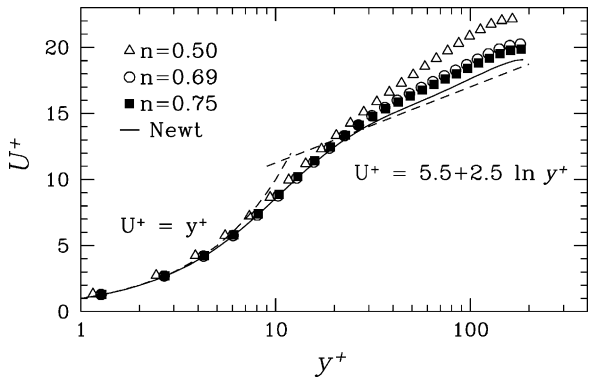

Fig. 4. Mean axial velocity profiles for the turbulent flow of three different power law fluids at $Re_g \approx 5500$ ($n = 0.5$, 0.69 and 0.75). The profiles have been non-dimensionalised using the conventional non-dimensionalisation with the mean wall viscosity taking the place of the Newtonian viscosity. Shown for comparison is a correlation for low Reynolds number turbulent pipe flow (dashed line) and DNS results at $Re = 5500$ (solid line), both for a Newtonian fluid.

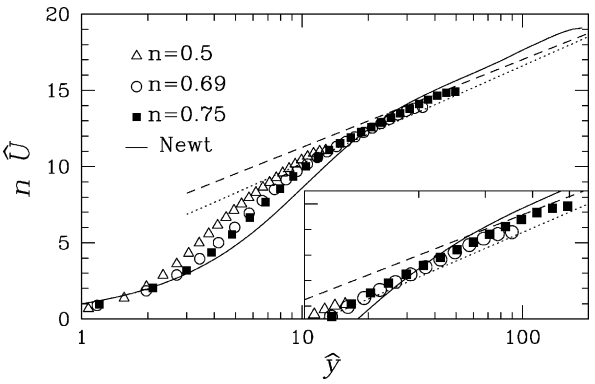

Fig. 5. Mean axial velocity profiles for three different power law fluids for $Re_g \approx 5500$, plotted using Clapp's non-dimensionalisation, and compared to the Newtonian profile at $Re = 5500$. The dotted line is Clapp's correlation using his coefficients ($A = 3.8$, $B = 2.78$) and the dashed line is using the generally accepted values for low Reynolds number Newtonian flow ($A = 5.5$, $B = 2.5$).

the turbulent flow of power law fluids is a function of the flow index, n, and satisfies

$$\hat{U} = \frac{A}{n} + \frac{B}{n} \ln \hat{y}, \tag{9}$$

where

$$\hat{y} = \left[\frac{(\varrho^n \tau_w^{2-n})^{1/2}}{K} \right] y^n \tag{10}$$

and $\hat{U}$ is the same as U^+ introduced in Section 2.1. The values of the parameters in Eq. (9) given by Clapp are $A = 3.8$ and $B = 2.78$, and were chosen to give collapse to the experimental measurements of a Newtonian fluid ($n = 1$) reported in [22]. The values of these coefficients for well-developed turbulent flow of Newtonian fluids are now generally accepted to be $A = 5.0$, $B = 2.5$ (while for low Reynolds number flow, $A = 5.5$ gives a closer fit to the data [24]). Thus it may be expected that $A = 5.5$, $B = 2.5$ should now replace the values used by Clapp in [21].

In Fig. 5 the mean axial velocity (multiplied by n) is compared to Clapp's correlation [21]. The dotted line is the logarithmic profile using the coefficients $A = 3.8$, $B = 2.78$ while the dashed line uses $A = 5.5$, $B = 2.5$. Clearly seen in this figure is that the DNS results for all three flow indices collapse to a similar profile and agree quite well with the general form of Clapp's correlation—they fall between the dotted and dashed lines for $\hat{y} > 10$. Clapp's correlation has drawbacks, in particular the velocity gradient predicted at the pipe centre is non-zero, and other correlations exist that include better approximations for the turbulent core [23]. However, Eq. (9) has the benefit that it is easy to calculate. The results here suggest that it is applicable, and perhaps for a wider range of flow indices than Clapp's experiments, although the original coefficients should probably be modified in light of more recent turbulence measurements in Newtonian fluids.

3.1.2. Turbulence statistics

Turbulence intensities, turbulence production, Reynolds shear stresses and rms streamwise vorticity fluctuations are plotted in Fig. 6 in physical coordinates and in Fig. 7 in wall units.

For both the axial turbulence intensities and the Reynolds stresses, the results for the power law fluids are close to the Newtonian results (DNS at $Re = 5500$). However, for both radial and azimuthal velocity fluctuations, the values for the power law fluids are significantly lower than the Newtonian case, and decrease with decreasing n. This behaviour has been observed experimentally [1,3] in turbulent flow of non-Newtonian fluids, although there is no clear understanding of why the relative magnitudes of the axial and in-plane velocity fluctuations are different.

Similar behaviour is also found in measurements of low Reynolds number Newtonian turbulence. Low and high Reynolds number flows produce almost identical (non-dimensionalised) axial velocity fluctuations, whereas the transverse components are weaker for low Reynolds number and have their peak somewhat closer to the pipe wall [24]. Thus these phenomena in the shear-thinning results are possibly features of flows that are not fully developed and in which a self-similar velocity profile is not yet established in the pipe. Because the viscosity is higher in the core region (in the shear-thinning case), the turbulence is not as fully developed there, especially for the fairly low generalised Reynolds number of 5500 used in the simulations here. Consequently, lower transverse fluctuations might be expected in shear-thinning fluids in the core region simply because of this under-development.

The results in [10] suggest that as Re_g increases, the transverse velocity fluctuations do increase, although it is not clear if the gap between them and the Newtonian results will be bridged or not. It appears possible that the increased viscosity in the core regions of the flow in shear-thinning fluids may always result in lower fluctuations than in a

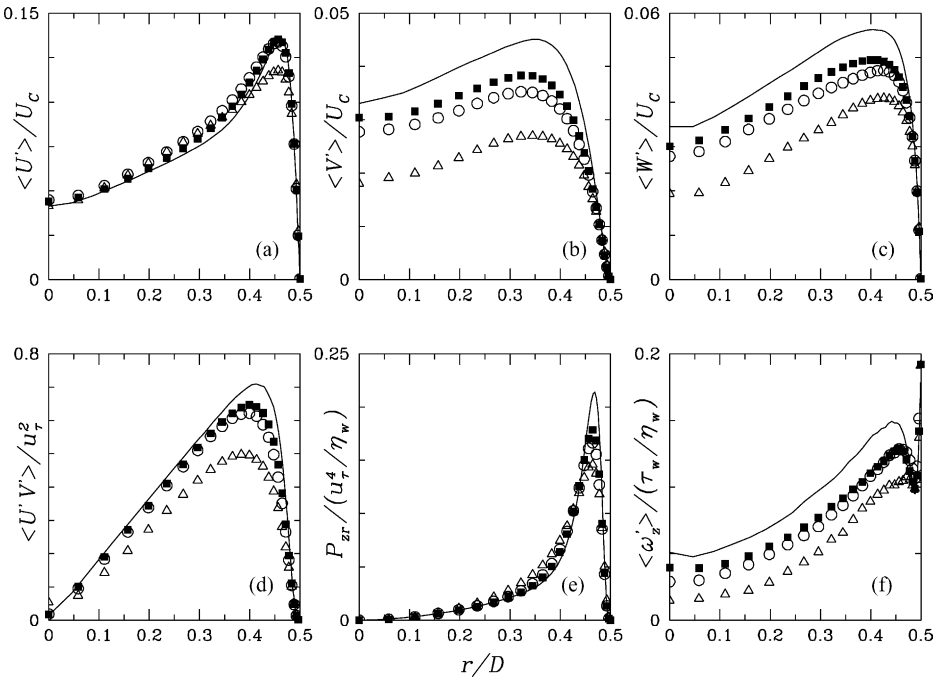

Fig. 6. Turbulence intensities: (a) axial, (b) radial and (c) azimuthal, (d) Reynolds shear stress, (e) turbulence production, and (f) rms axial vorticity fluctuation plotted as a function of r/D. (Solid line for Newtonian DNS, power law fluids are $n = 0.5$ (△), $n = 0.69$ (○) and $n = 0.75$ (■).

Newtonian fluid, although conclusive evidence must await further work at higher Re_g. As $n \rightarrow 1$ in Fig. 6, the non-Newtonian results approach the Newtonian correlations, as expected.

The distance from the wall of the peak velocity fluctuations and Reynolds stress generally decreases as the flow index decreases (although the peak of the radial fluctuation increases somewhat in non-dimensional units, Fig. 7b). This is a reflection of the increased viscosity away from the wall that damps out turbulent fluctuations. The production of turbulence is given by

$$P_{zr} = \overline{U'V'}\frac{\partial \bar{U}}{\partial r} \tag{11}$$

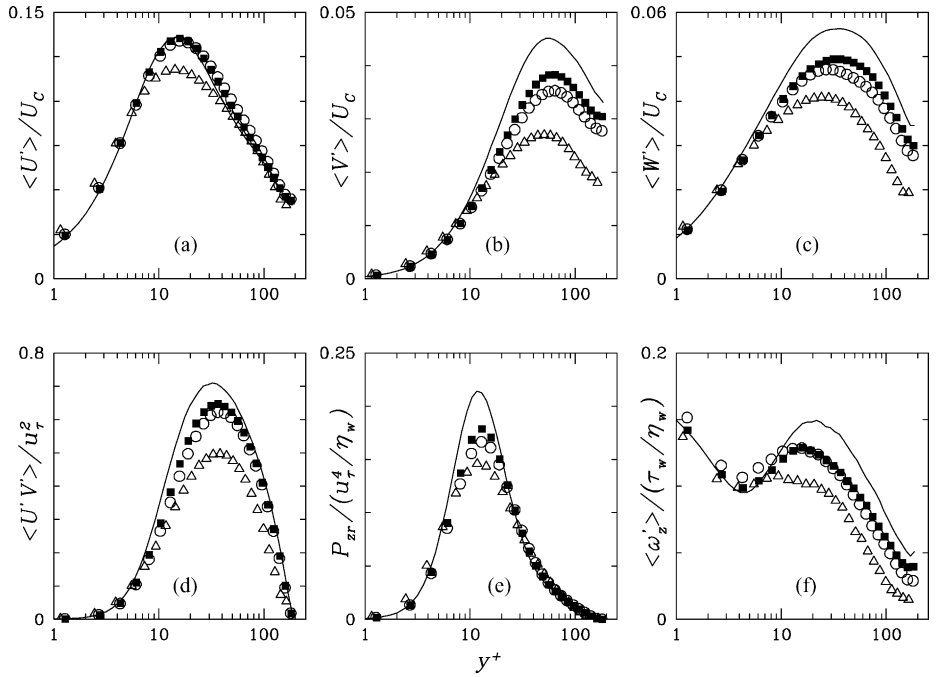

Fig. 7. As for Fig. 6 plotted in wall coordinates.

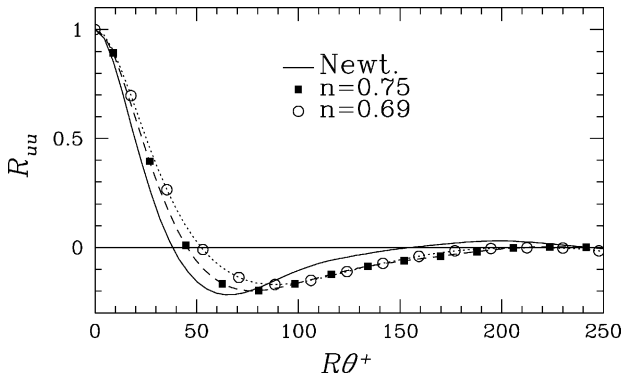

Fig. 8. Azimuthal two-point correlation of the fluctuation velocity $R_{uu} = \langle U'(\theta)U'(\theta + \delta\theta)\rangle$ at $y^+ = 20$. The mean streak spacing is estimated as twice the value of separation at the minimum value of R_{uu}.

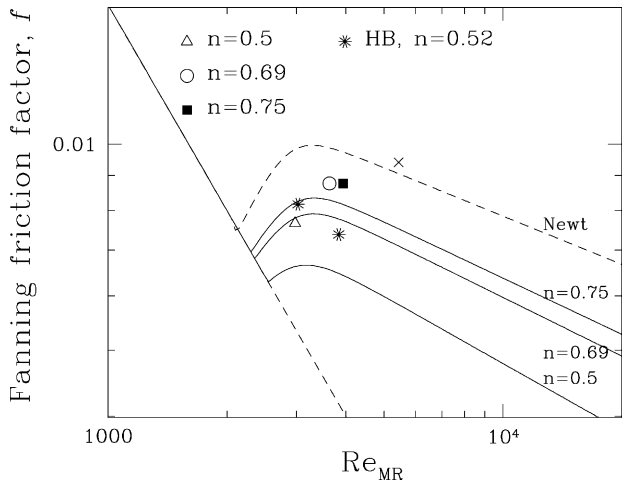

Fig. 9. Fanning friction factors determined for the DNS simulations as a function of the Metzner–Reed Reynolds number. The Herschel–Bulkley results are denoted by ∗ and DNS results of a Newtonian fluid at $Re = 5500$ denoted by ×.

and is plotted in Figs. 6e and 7e. As seen, the maximum production occurs at a value of $y^+ \approx 10$ for the Newtonian fluid. For the power law fluids this distance increases slightly for $n = 0.75$ and 0.69, decreasing slightly for $n = 0.5$, although the differences are small. The rms fluctuation of the streamwise vorticity is plotted in Figs. 6f and 7f. They show slightly lower peak values as n decreases, with the location of the peak slightly closer to the wall than in the Newtonian case, consistent with the velocity fluctuation results. The mean wall streak spacing for the simulations was determined from the azimuthal two-point correlation of the fluctuating axial velocity ($R_{uu} = \langle U'(\theta)U'(\theta + \delta\theta)\rangle$), shown in Fig. 8. The streak spacing for the Newtonian simulation is approximately 125 wall units, for $n = 0.75$ it is 155 wall units and for $n = 0.69$ it is 180 wall units, suggesting larger streamwise vortices as n decreases, although their intensity becomes weaker with decreasing n. It was not possible to estimate a reliable streak spacing from the $n = 0.5$ results.

3.1.3. Comparison to visco-elastic DNS results

It is interesting to compare the shear-thinning results here to those for visco-elastic fluids presented in [5–7]. In those studies, the conclusion was drawn that polymer additives modify the turbulent structure in the buffer layer ($10 < y^+ < 30$) to increase the streamwise vortex size, lessen the streamwise vortex strength, and consequently supply less energy to the log layer. The reduction in advective transport of high-momentum fluid from the core toward the wall ultimately leads to the prediction of drag reduction. Correlated to the weaker vortices were reduced wall normal and spanwise velocity fluctuations compared to the Newtonian case (these correspond to radial and azimuthal fluctuations here). It was also observed that streamwise (axial) velocity fluctuations were slightly higher than the Newtonian case. As the degree of visco-elasticity increased, these trends increased and it was seen that the mean velocity log-layer slope increased also.

The description of the majority of these phenomena are similar in character to those observed here when ‘degree of visco-elasticity’ is replaced by ‘degree of shear-thinning’. Recall that results presented here are for a fluid that is purely shear-thinning. The major differences between the shear-thinning results and the visco-elastic results are that the axial velocity fluctuations decrease with shear-thinning (they increase with visco-elasticity) and the peak values of the velocity fluctuations occur closer to the wall in the shear-thinning case, not further away. Both of these predictions are consistent with an increase in viscosity away from the wall (and hence enhanced viscous damping) that occurs in shear-thinning fluids. A final comment regarding Fig. 7 is that the similarity in shape of the profiles and the location of maxima between the shear-thinning fluids and the Newtonian case suggest that non-dimensionalisation based on the mean wall viscosity η_w is appropriate, and hence use of Re_g as a basis for comparison is justified.

3.1.4. Friction factors

The Fanning friction factor, f, is defined as the non-dimensional wall shear stress and is defined as

$$f = \frac{\tau_w}{(1/2)\rho\bar{U}^2}. \tag{12}$$

For shear-thinning fluids, the friction factor is traditionally plotted against the Metzner–Reed Reynolds number (Eq. (7)). The results obtained numerically here are compared in Fig. 9 to the friction factors determined by Dodge and Metzner [13].

The numerical results predict friction factors that are lower than the corresponding values for a Newtonian fluid. Qualitatively they agree with experimental observations [13] in which shear-thinning behaviour was seen to lead to a reduction in friction factor for a fixed Re_{MR}. Quantitatively, it is clear that the predicted values from simulation are higher than those measured in [13] by approximately 10–15%—the reason for this difference is unclear, although

it is likely that the fluids used in [13] were not well represented as power law fluids over the range of shear rates applicable to their turbulent flow. The possibility of numerical inadequacies remains, although validation work, grid convergence studies and a domain length study (reported below, in which doubling the domain length modified the friction factor by less than 2%) all suggest that this is not likely to be a major factor.

3.1.5. Intermittency and transition for power law fluids

Time traces of velocity and pressure signals for $n = 0.5$ and 0.75 are shown in Fig. 10. Traces at the centreline (dashed line) and near-wall (solid line) are shown, although are difficult to distinguish except for the case of the axial velocity component, U. There is a clear distinction between the results for the two different flow indices. The signals for $n = 0.75$ (lower three graphs) appear as a fairly random perturbation around a mean value, whereas the signals for $n = 0.5$ (upper three graphs) are clearly showing large-scale coherent excursions with a random signal superimposed.

The period of these large deviations is found to be approximately equal to the length of the computational domain ($4\pi D$) divided by the centreline velocity—hence these results are a computational artefact and cannot be relied on as an accurate representation of the real flow for the case of $n = 0.5$. The axial extent of these structures is significantly less than the domain length (approximately half, see contours of the axial velocity near the pipe wall in Fig. 11) yet they are self-sustaining over many transit times of the domain. This result suggests that the flow is likely to be transitional and in reality will contain intermittent phenomena.

Fig. 11 shows that for the case of $n = 0.5$ (top panel), a large region of turbulent activity exists toward the left of the domain whereas the region near the centre of the flow is fairly devoid of unsteady structure. This type of flow shows typical transitional behaviour and is similar to the turbulent puffs observed in Newtonian fluids in the transitional regime, although it occurs here at a generalised Reynolds number that is quite high compared to Newtonian transition. In the simulation, the active region of the flow continually moves

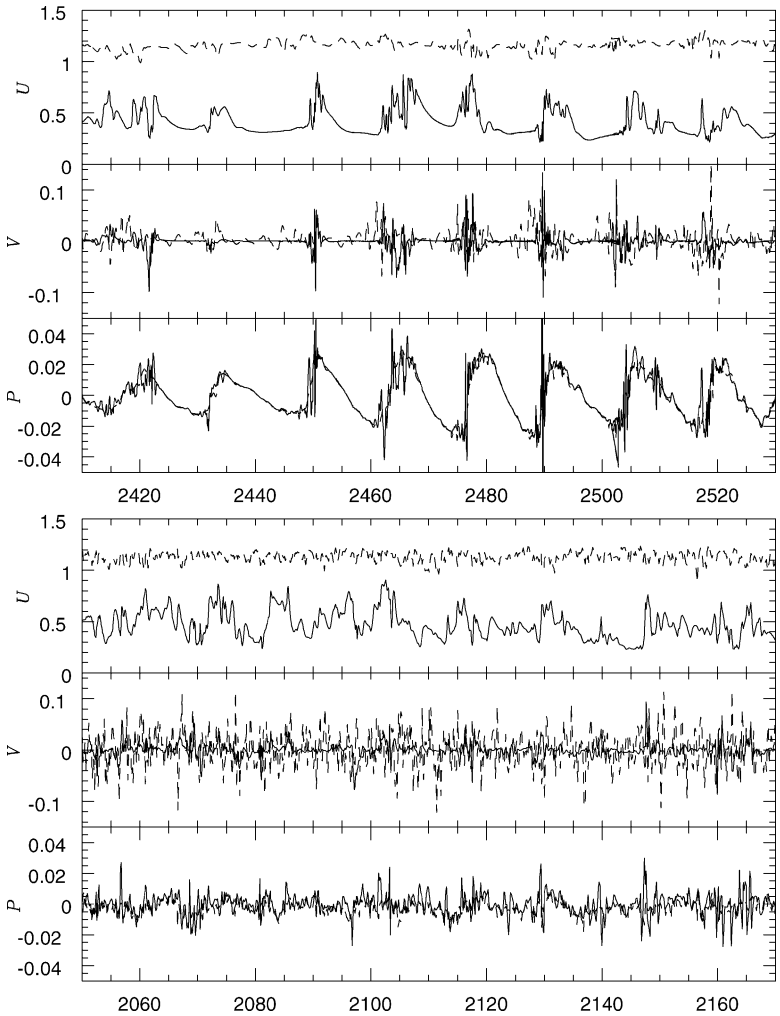

Fig. 10. Time traces of axial velocity, radial velocity, and pressure near the wall (solid line) and near the pipe centre (dashed line) for $n = 0.5$ (top three graphs) and $n = 0.75$ (bottom three graphs). All units are non-dimensionalised.

along the pipe and appears to preferentially occur at one azimuthal location for extended times, so that the average velocity profile over approximately 10 domain transit times (100 pipe diameters) shows some asymmetry. This suggests that permanent asymmetry might be able to be sustained in the transitional regime for power law fluids if a preferential mechanism exists for triggering the puffs (for example, an upstream pipe bend), and may explain the asymmetry observed in experiments in [3]. Because of the short domain, this possibility is purely speculative although it warrants a more detailed study. The $n = 0.5$ case has been re-run with a domain length that is twice as long (results are discussed in a subsequent section).

As the flow index increases, the distribution of wall streaks becomes more homogeneous in Fig. 11, although there are still local structures for both $n = 0.69$ and 0.75. In each case, the wall streaks are quite long, further suggesting that the flow is not fully developed for any of the three power law fluids at this Re_g. However, the time series for $n = 0.69$ and 0.75 do not show large-scale time coherence, indicating that these flows are of a fundamentally different character to the case of $n = 0.5$ which can be categorised as transitional. For the case of $n = 1$ (a Newtonian fluid) the structure is more random and the streaks shorter, indicative of more developed turbulence. These results taken together are evidence that transition is delayed for more shear-thinning fluids under the assumption that Re_g is a valid basis for comparing them.

Instantaneous snapshots of axial velocity, cross-sectional velocity, and contours of viscosity for $Re_g \approx 5500$ are shown in Fig. 12. These cross-sections are taken at an axial location that is inside the intense turbulent structure seen in $n = 0.5$ in Fig. 11 and highlight the most unsteady regions in the pipe. The contour scales are identical for each flow index and the magnitude of the cross-sectional velocity scales are also equal. They show the degree of unsteadiness in the flow as well as the degree to which the major unsteady structures are confined to regions close to the pipe wall for the power law fluids, whereas there is a significantly increased degree of structure in the core region of the Newtonian fluid.

Clearly seen are lower viscosities (indicative of higher shear rates) in the wall regions of the power law viscosity contour plots. A plot of the mean viscosity as a function of radius for the three power law simulations is given in Fig. 13. Of note is the range of viscosities, with a relatively small difference in mean viscosity between wall and centreline for $n = 0.75$ (a factor of approximately 2), whereas a factor of approximately 4.6 applies for $n = 0.5$. This difference is also seen in the instantaneous viscosity plots in Fig. 12 where the higher viscosities (seen as dark contours) are quite prominent. This behaviour is expected because for

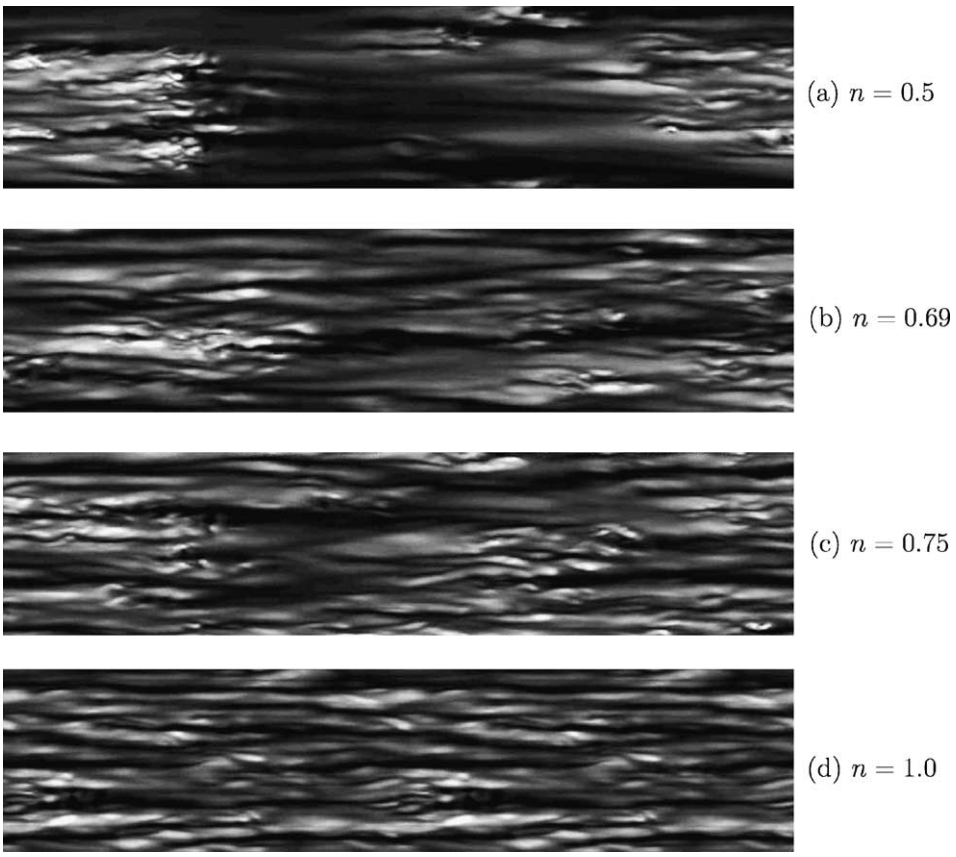

Fig. 11. Contours of instantaneous axial velocity close to the pipe wall for power law fluids, $Re_g \approx 5500$, $n = 0.5$ (top), 0.69, 0.75 and Newtonian fluid ($Re = 5500$) (bottom). (The data extraction surface has been rolled flat and the flow is from left to right. White represents high velocity and black low.)

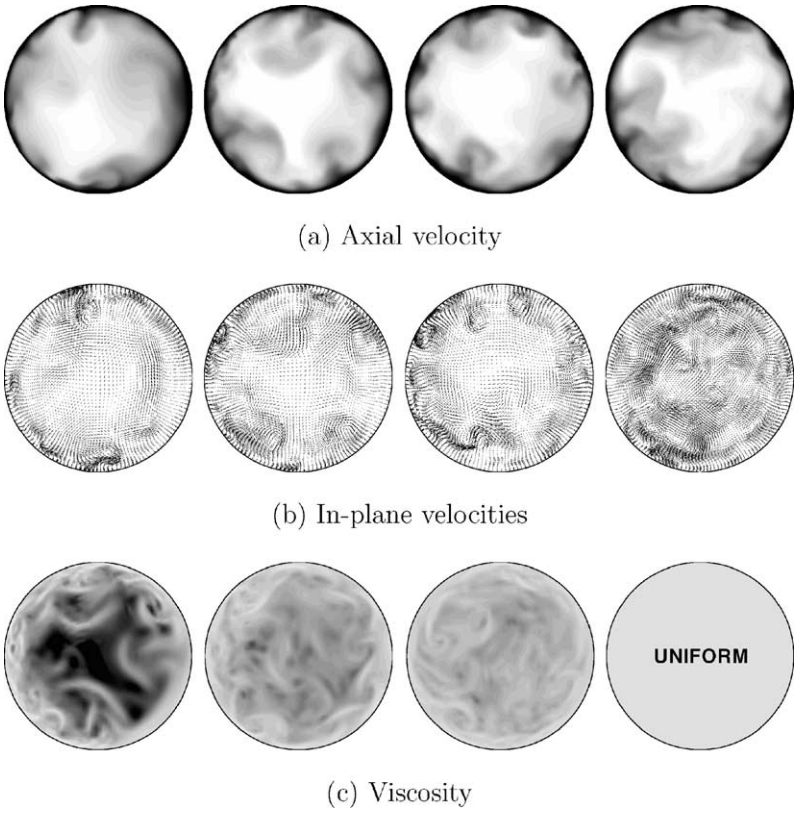

Fig. 12. Contours of instantaneous axial velocity, in-plane velocity vectors, and viscosity for power law fluids, all for $Re_g \approx 5500$ and $n = 0.5$ (left), 0.69, 0.75 and Newtonian fluid ($Re = 5500$) (right). (For axial velocity, white contours are high and black low. For viscosity, white is low viscosity and black high.)

more shear-thinning fluids, with the same value of mean wall viscosity, higher core viscosities are inevitable. The mean viscosity averaged over the domain for the three power law cases is 3.35, 1.86 and 1.49 times the wall viscosity for $n =$ 0.5, 0.69 and 0.75, respectively.

3.1.6. Results for extended domain with $n = 0.5$

As discussed above, the simulation for $n = 0.5$ was in a transitional regime and the observation of a puff-type structure that persisted for many domain transit times was possibly a numerical artefact. Consequently, this simulation was run on a domain with length $8\pi D$ (twice as long) with twice the number of axial mesh points (i.e. at the same axial resolution). To initialise this simulation, one half of the domain was set equal to the $4\pi D$ solution at a given time and the remaining half set to the solution at one axial location in an inactive part of the pipe (so that the solution varied smoothly along the entire domain length). The importance of this initial condition is that it contained only one large turbulent structure, whose evolution could be compared to the shorter domain results. This simulation was run for approximately 12 domain transit times (over 300 pipe diameters), with average statistics being collected over the last six domain transit times.

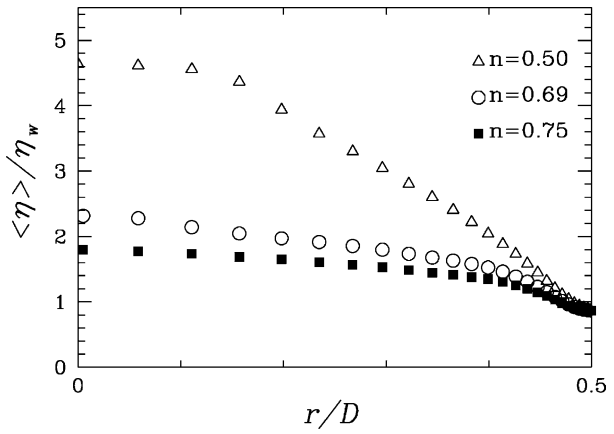

Fig. 13. Mean normalised viscosity as a function of radius for power law fluids at $Re_g \approx 5500$.

A comparison of the average flow results for the two different domain lengths is presented in Fig. 14. As can be seen, the results are very similar, the major difference being in the axial turbulence intensity that is slightly higher for the longer domain length.

The character of the near-wall structure is shown in Fig. 15 (cf. Fig. 11a for the shorter domain). There is some difference in structure in that the single large puff that fills the cross-section (and which lasts for many transit times of the short domain) breaks down in the longer domain to form a number of smaller structures. These structures continually

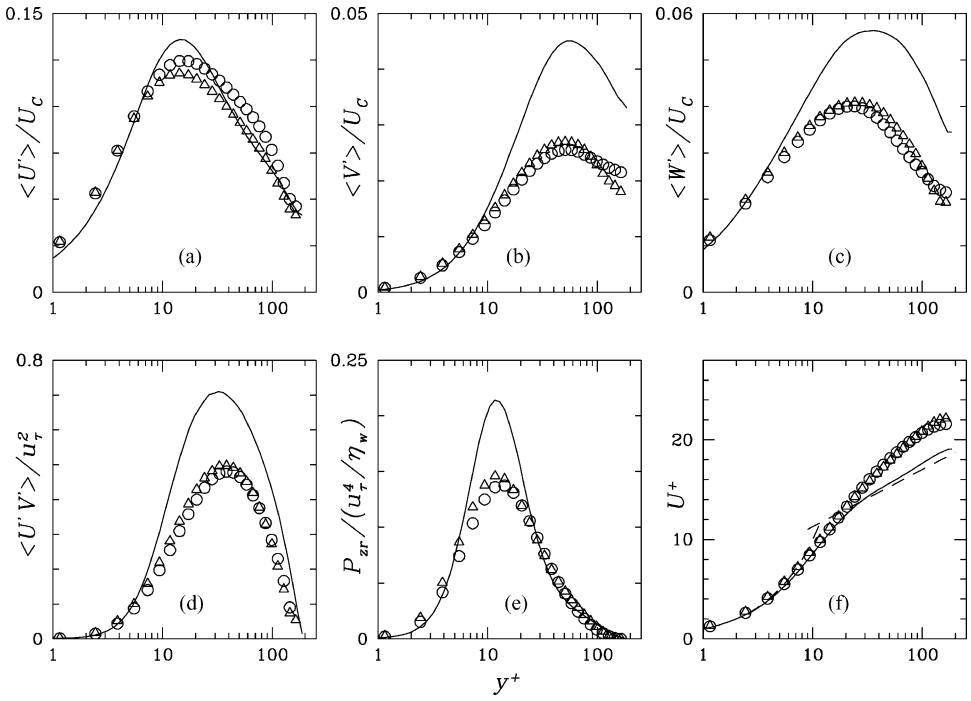

Fig. 14. Turbulence intensities: (a) axial, (b) radial and (c) azimuthal, (d) Reynolds shear stress, (e) turbulence production, and (f) mean wall velocity profile for the case $n = 0.5$. (Solid line for Newtonian DNS, domain length $4\pi D$ (△), $8\pi D$ (○).)

break and merge, although it is clear that they do not fill the domain even after travelling the equivalent of 300 pipe diameters. The assessment of this flow as transitional continues to be supported by the extended domain results. The friction factor determined from these results differs from the shorter domain calculation by less than 2%.

3.2. Results for the Herschel–Bulkley fluid

Results for the Herschel–Bulkley fluid are preliminary and two simulations have been run for one fluid rheology and two values of Re_g (for parameters see Table 1). Rheology values were chosen to match experimental results for a 0.05 wt.% Ultrez 10 solution and were estimated from a curve fit to a rheogram obtained in a Bohlin rheometer. The fit gave a yield stress of $\tau_y = 1.35$ Pa, a consistency $K = 1.203$ and a flow index $n = 0.52$. The experimental measurements indicated that a pressure gradient of 1.42 kPa/m resulted in a superficial velocity of 3.36 m/s in the line (ID of 105 mm) and a generalised Reynolds number of $Re_g = 7027$.

When the same values as the experiment are used in the simulation, the superficial velocity predicted by the simulation is 11% lower than the measured value and the predicted Re_g is 5800 (the discrepancy is larger than 11% because both the superficial velocity and the mean wall viscosity are different). A second simulation was run at a higher pressure gradient (1.75 kPa/m) and resulted in a superficial velocity of 3.5 m/s and $Re_g = 8130$. The Re_g of the two simulations bracketed the Re_g of the experimental measurements. The computationally predicted profiles (in conventional wall units based on the mean wall viscosity) are presented in Fig. 16.

The simulation results show good general agreement in terms of shape and magnitude when compared to the

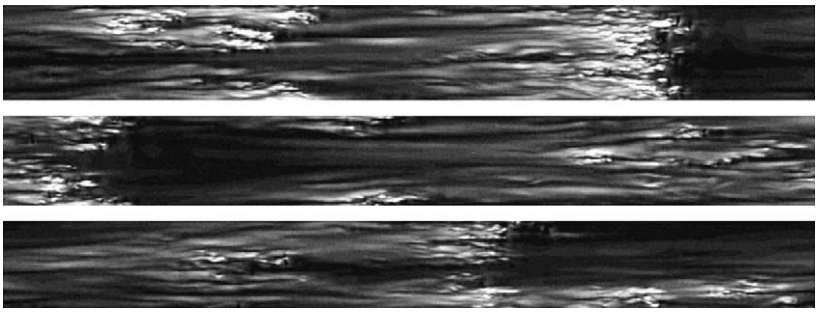

Fig. 15. Contours of instantaneous axial velocity close to the pipe wall for $n = 0.5$ at three times. Each image is separated by approximately two domain transit times (equivalent to 50 pipe diameters between consecutive images).

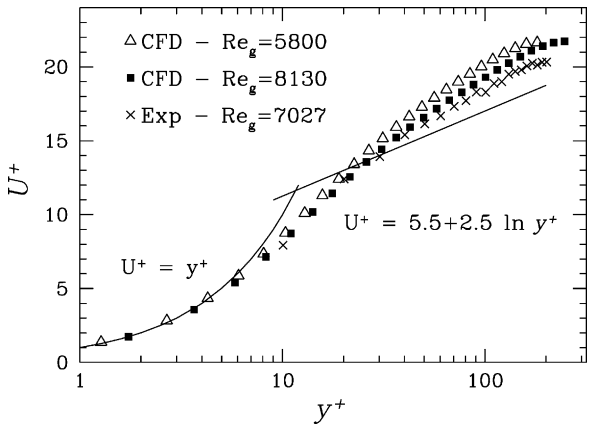

Fig. 16. Mean axial velocity profile in conventional (Newtonian) wall units for a Herschel–Bulkley fluid: comparison of DNS results at $Re_g = 5800$ (△), $Re_g = 8130$ (■) and experimental results at $Re_g = 7027$ (×).

experimentally measured profile. The velocity profiles for both simulations lie slightly above the low Reynolds number Newtonian profile, indicating that either the flow is less well developed than that of a Newtonian fluid at similar Reynolds numbers or that there is a fundamentally different turbulent structure in the case of a yield stress fluid. Note that the DNS profiles do not bracket the experimental profile, despite the simulation Re_g bracketing the Re_g of the experiment. Both DNS profiles lie slightly above the experimental one, suggesting that there is a difference between the flow of a 'pure' Herschel–Bulkley fluid (as approximated in the simulations) and the flow of the model fluid used in the experiments. This is not surprising given that the rheology is a curve fit obtained over a limited range of shear rates. However, the discrepancy between DNS and measurement is significantly less than that observed for the power law experiments discussed in Section 2.2.1 (and reported in [9,10]) and suggests that elastic and elongational viscosity effects are not important for the real fluid and furthermore that the Herschel–Bulkley model is a reasonable approximation for the experimental fluid over the range of shear rates present in the flow.

Turbulence statistics are shown in Fig. 17. Good agreement between the simulated and measured axial and azimuthal turbulence intensities is seen in Fig. 17a and c. Turbulence intensities and Reynolds stresses follow the same trend as the results for the power law fluids (see Fig. 7), and the results for the $Re_g = 5800$ Herschel–Bulkley simulation have very similar shapes and magnitudes to those for the power law simulation for $n = 0.5$. This suggests that a small yield stress (as simulated here) has very little effect on the second-order turbulence statistics. The major difference between the Herschel–Bulkley and power law results is in the location of maximum turbulence production that is shifted to $y^+ \approx 16$ for the lower Re_g flow of the yield stress material. The results in Figs. 16 and 17 are encouraging and suggest that DNS is able to provide reliable predictions of the turbulent flow of shear-thinning fluids provided an appropriate choice of rheological model is made.

Near-wall structures are shown in Fig. 18 and cross-sections of velocity and viscosity are presented in Fig. 19. The DNS results predict that this flow is also transitional

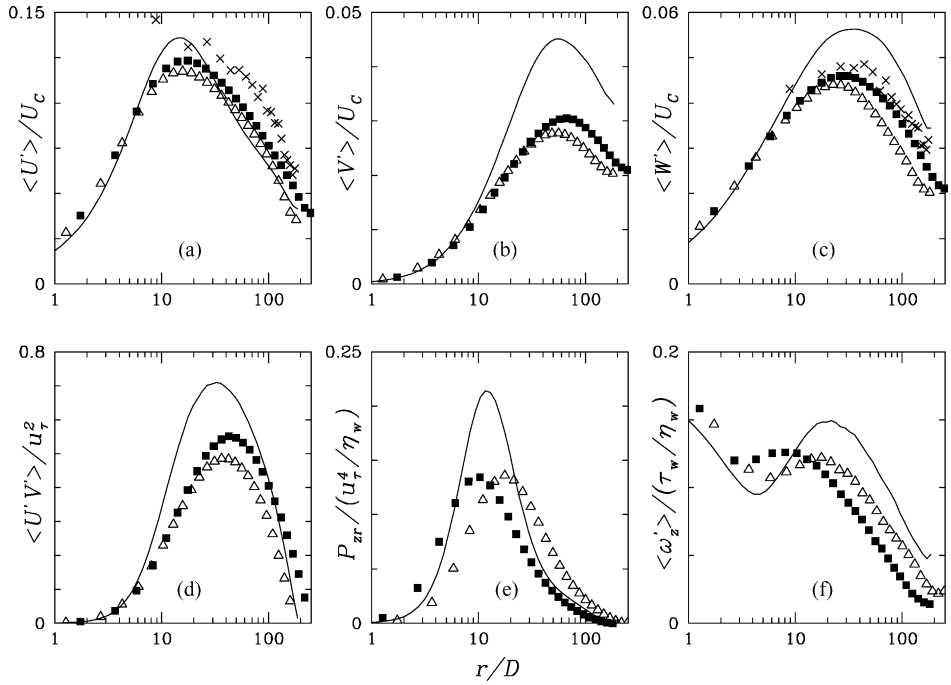

Fig. 17. Turbulence intensities: (a) axial, (b) radial and (c) azimuthal, (d) Reynolds shear stress, (e) turbulence production, and (f) rms axial vorticity fluctuation plotted as a function of y^+ (solid line is Newtonian DNS at $Re = 5500$). Herschel–Bulkley simulations are $Re_g = 5800$ (△) and $Re_g = 8130$ (■). Experimental results (where available) are (×).

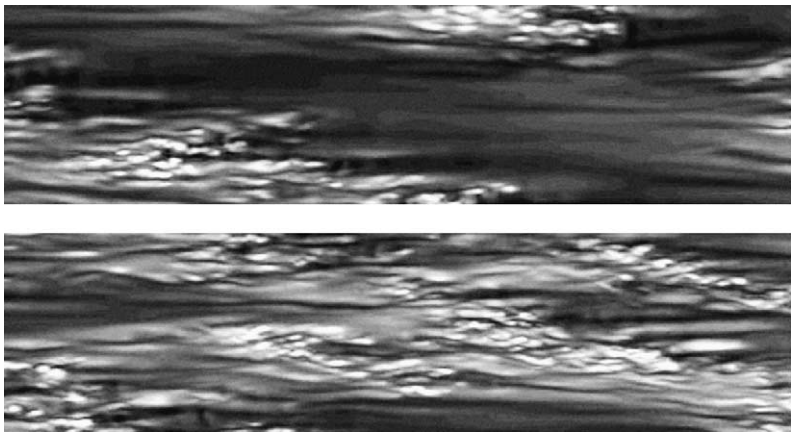

Fig. 18. Contours of instantaneous axial velocity close to the pipe wall for the Herschel–Bulkley fluid at $Re_g = 5800$ (top) and $Re_g = 8130$ (bottom). The data extraction surface has been rolled flat and the flow is from left to right. White represents high velocity and black low.

at the lower Re_g, with slug/puff type behaviour predicted (see Fig. 18). As in the case of the $n = 0.5$ power law simulation, it was not possible to determine a reliable estimate of the near-wall streak spacing from these results. The structures and general appearance of these images is similar to the $n = 0.5$ power law results, and for the comparatively low yield stress utilised in the simulations there are no significant differences between the two fluid types. Additional simulations for different flow indices and for a wider range of yield stresses need to be undertaken to more fully explore the effect of yield stress.

The mean viscosity as a function of radius (normalised by the wall viscosity) is shown in Fig. 20. The difference between the mean wall and centreline viscosity for $Re_g = 5800$ is approximately 7, and for $Re_g = 8130$ it is 8, showing that the presence of a yield stress has had a measurable influence on the viscosity profile (compare to the centreline to wall viscosity ratio of approximately 5.4 for the power

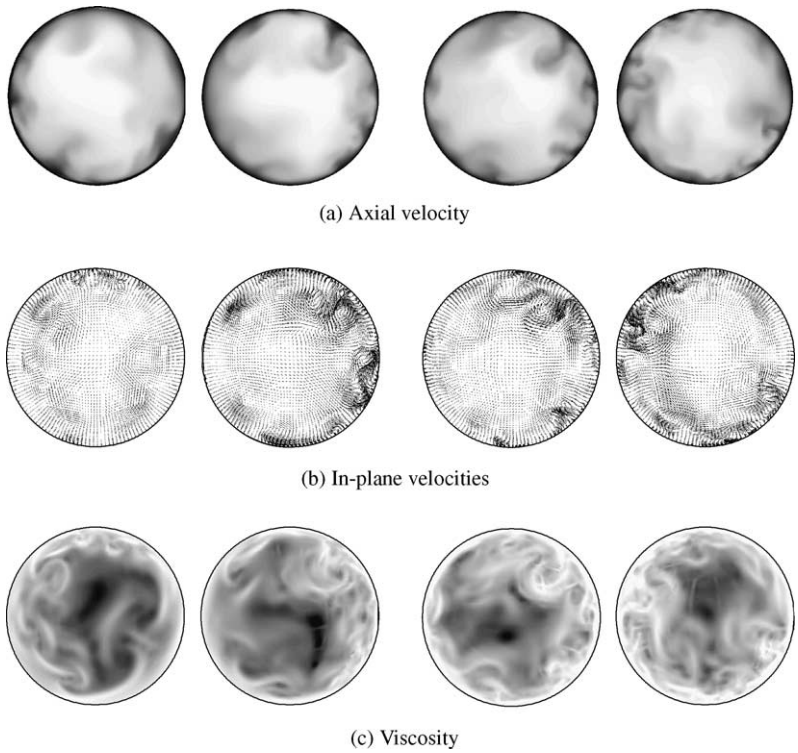

Fig. 19. Contours of instantaneous axial velocity, in-plane velocity vectors, and viscosity for power law fluids. The two columns on the left are different axial locations for $Re_g = 5800$ and the two columns on the right are for $Re_g = 8130$. (For axial velocity, white contours are high and black low. For viscosity, white is low viscosity and black high.)

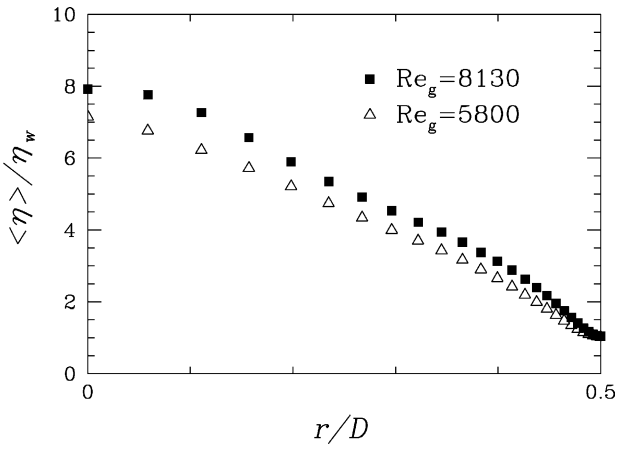

Fig. 20. Mean normalised viscosity as a function of radius for Herschel–Bulkley fluids at two different Re_g.

simulation at a similar Re_g). Interesting to note is that the higher Re_g case has a greater ratio of centreline to wall viscosity, although the actual magnitudes of viscosity are smaller for the higher Re_g case.

4. Summary of results

The applicability of Clapp's scaling and log law for power law fluids is backed up by the present DNS results for power law fluids, although the Reynolds numbers used here are lower than those used to derive the experimental correlation. The parameters used by Clapp ($A = 3.8$, $B = 2.78$) should probably be modified so that they collapse to the generally accepted values for Newtonian turbulence. The results also suggest that as the power law index (n) is decreased, and the deviation from Newtonian rheology increases, the value of Re_g at which transition occurs will also increase. The results shown here (in particular, in Figs. 6–8) suggest that use of the wall viscosity (Eq. (5)) and the generalised Reynolds number (Eq. (6)) are a suitable basis on which to non-dimensionalise and compare the flows of generalised Newtonian fluids.

The friction factors predicted by the simulations are 10–15% higher than the Dodge and Metzner correlations obtained from experiment and presented in [13]. This is most likely related to the imperfect fit of the experimental fluids with power law rheology. However, the simulation results here show that a reduction in the friction factor results for shear-thinning (non-visco-elastic), power law fluids, and is consistent with experimental results. The reduction in friction factor is due to the higher core viscosities that reduce the strength of the near-wall eddies, and hence momentum transfer from the core to the wall. Direct comparison of friction factors for different n is complicated because a consistent reference state is not introduced given the different viscosity levels in the core of the flow for different cases.

The results are supportive of a transition mechanism for shear-thinning fluids that is similar to Newtonian fluids and which occurs via intermittency and turbulent events like the slugs and puffs. Although there was some difference in the extent of these structures when the domain length of the simulation was increased, isolated structures persisted in the simulation for many domain transit times. These unsteady structures may potentially be able to resuspend small settling particles in particle-laden flows, allowing the transitional regime to be possible for suspension transport in power-law carrier fluids. Because the specific energy consumption of hydraulic conveying is lowest at transition, transport in this regime has the additional benefit of being the most energy efficient, and design based on flow rates and rheology could be undertaken to choose the transitional regime.

Simulations of a Herschel–Bulkley fluid were in quite good agreement compared to Ultrez 10 experimental results. They also showed similar behaviour to the power law simulation results, with log-law profiles that lay above the Newtonian profile (suggesting undeveloped flow) and velocity fluctuations with similar behaviour. Like the power law results, the flow had some of the character of a transitional flow.

Difficulties encountered in experimentation as a result of using polymer solutions to approximate idealised rheologies can lead to problems of interpretation and understanding. The application of DNS to flows of non-Newtonian fluids with certainty of the rheology being studied has the potential to enable the effect of different rheological parameters to be correctly quantified and understood. This is possibly the greatest contribution that DNS can bring to the study of flows of non-Newtonian fluids. However, given the difficulty in approximating a measured rheology over a very wide range of shear rates using any of the simple generalised Newtonian rheology models, it appears likely that obtaining accurate results of turbulent flow of real non-Newtonian fluids using DNS will remain a difficult task.

Acknowledgements

The authors gratefully acknowledge the support of AMIRA, BHP-Billiton, De Beers, Rio Tinto, WMC Resources Limited and Warman International (via AMIRA project P599) for partial sponsorship of the work described in this paper.

References

[1] F.T. Pinho, J.H. Whitelaw, Flow of non-Newtonian fluids in a pipe, J. Non-Newtonian Fluid Mech. 34 (1990) 129–144.
[2] M.P. Escudier, F. Presti, Pipe flow of a thixotropic liquid, J. Non-Newtonian Fluid Mech. 62 (1996) 291–306.
[3] M.P. Escudier, F. Presti, S. Smith, Drag reduction in the turbulent pipe flow of polymers, J. Non-Newtonian Fluid Mech. 81 (1999) 197–213.
[4] R. Sureskumar, A.N. Beris, A.H. Handler, Direct numerical simulation of the turbulent channel flow of a polymer solution, Phys. Fluids 9 (1997) 743–755.

[5] C.D. Dimitropoulos, R. Sureshkumar, A.N. Beris, Direct numerical simulation of viscoelastic turbulent channel flow exhibiting drag reduction: effect of the variation of rheological parameters, J. Non-Newtonian Fluid Mech. 79 (1998) 433–468.
[6] A.N. Beris, C.D. Dimitropoulos, Pseudospectral simulation of turbulent viscoelastic channel flow, Comput. Meth. Appl. Mech. Eng. 180 (1999) 365–392.
[7] E. De Angelis, C.M. Casciola, R. Piva, DNS of wall turbulence: dilute polymers and self-sustaining mechanisms, Comput. Fluids 31 (2002) 495–507.
[8] M.R. Malin, Turbulent pipe flow of power-law fluids, Int. Comm. Heat Mass Transf. 24 (1997) 977–988.
[9] M. Rudman, H.M. Blackburn, L.J.W. Graham, L. Pullum, Weakly turbulent pipe flow of a power law fluid, in: Proceedings of the 14th A/Asian Fluid Mechanics Conference, Adelaide, 2001.
[10] M. Rudman, L.J.W. Graham, H.M. Blackburn, L. Pullum, Non-Newtonian turbulent and transitional pipe flow, in: Hydrotransport 15, Banff, 2002.
[11] A.A. Draad, G.D.C. Kuiken, F.T.M. Nieuwstadt, Laminar-turbulent transition in pipe flow for Newtonian and non-Newtonian fluids, J. Fluid Mech. 377 (1998) 267–312.
[12] P.K. Ptasinski, F.T.M. Nieuwstadt, B.H.A.A. Van den Brule, M.A. Hulsen, Experiments in turbulent pipe flow with polymer additives at maximum drag reduction, Flow. Turb. Combust. 66 (2001) 159–182.
[13] D.W. Dodge, A.B. Metzner, Turbulent flow of non-Newtonian systems, AIChEJ 5 (1959) 189–204.
[14] G.E. Karniadakis, Spectral element–Fourier methods for incompressible turbulent flows, Comp. Meth. Appl. Mech. Eng. 80 (1990) 367–380.
[15] G.E. Karniadakis, M. Israeli, S.A. Orszag, High-order splitting methods for the incompressible Navier–Stokes equations, J. Comput. Phys. 97 (1991) 414–443.
[16] G.E. Karniadakis, S.A. Orszag, V. Yakhot, Renormalization group theory simulation of transitional and turbulent flow over a backward-facing step, in: Galerpin, Orszag (Eds.), Large Eddy Simulation of Complex Engineering and Geophysical Flows, CUP, 1993, pp. 159–177.
[17] K.C. Wilson, A.D. Thomas, A new analysis of the turbulent flow of non-Newtonian fluids, Can. J. Chem. Eng. 63 (1985) 539–546.
[18] M. Rudman, H.M. Blackburn, Large eddy simulation of turbulent pipe flow, in: Proceedings of the Second International Conference on CFD in the Minerals and Process Industry, Melbourne, 1999.
[19] S. Schmidt, D.M. McIver, H.M. Blackburn, M. Rudman, G.J. Nathan, Spectral element based simulation of turbulent pipe flow, in: Proceedings of the 14th A/Asian Fluid Mechanical Conference, Adelaide, 2001.
[20] S. Schmidt, H.M. Blackburn, Spectral element filtering techniques for large eddy simulation with dynamic estimation, J. Comput. Phys. 186 (2003) 610–629.
[21] R.M. Clapp, Turbulent heat transfer in pseudoplastic non-Newtonian fluids, in: Int. Dev. Heat Transfer, Part III, New York, 1961.
[22] R.G. Deissler, Investigation of turbulent flow and heat transfer in smooth tubes, including the effects of variable fluid properties, Trans. ASME 73 (1951) 101–107.
[23] A.V. Shenoy, D.R. Saini, A new velocity profile model for turbulent pipe-flow of power-law fluids, Can. J. Che., Eng. 60 (1982) 694–696.
[24] J.M.J. den Toonder, F.T.M. Nieuwstadt, Reynolds number effects in a turbulent pipe flow for low to moderate *Re*, Phys. Fluids 9 (11) (1997) 3398–3409.